View metadata, citation and similar papers at core.ac.uk
brought to you by CORE
provided by Elsevier - Publisher Connector

Conical Electron Tomography of a Chemical Synapse: Vesicles Docked to the Active Zone are Hemi-Fused

G. A. Zampighi,*‡ L. M. Zampighi,† N. Fain,* S. Lanzavecchia,§ S. A. Simon,¶** and E. M. Wright†
Departments of *Neurobiology, †Physiology, and ‡Jules Stein Eye Research Institute, University of California at Los Angeles School of Medicine, Los Angeles, California; §Department of Structural Chemistry, School of Pharmacy, University of Milan, Milan, Italy; and Department of ¶Neurobiology and **Center of Neuroengineering, Duke University Medical Center, Durham, North Carolina

ABSTRACT We have used thin sectioning and conical electron tomography to determine the three-dimensional structure of synaptic vesicles that were associated (docked) at release sites of the presynaptic membrane, called active-zones. Vesicles docked at the active zone occupied a strategic location: they formed regions of contact with the plasma membrane on one side and with that of one or more vesicles located deeper within the presynaptic terminal on the other side. The region of contact with the active zone measured ~15 nm in diameter (~2% of the vesicle's surface) and contained a smaller ~6 nm region where the proximal leaflets merged (hemi-fused). Hemi-fusion was only observed on the side of vesicles in contact with the active zone; at the side of contact between neighboring vesicles, the membranes were not hemi-fused. Approximately three-fourths of the docked vesicles contained hemi-fused regions. Vesicles fully fused to the active zone (exhibiting pores that appeared as interruptions of a single membrane) were less frequently observed (~1 of 10 hemi-fused vesicles). In conclusion, our observations in cortical synapses strengthen the hypothesis that hemi-fusion is a stable intermediary that precedes full fusion and release.

INTRODUCTION

A key feature of the current model of synaptic transmission holds that, upon electrical stimulation, single vesicles fuse at specific regions of the plasma membrane, called the active-zone, and release neurotransmitters stored in their lumens (1). Despite the success of the vesicular release model in explaining synaptic transmission, the series of steps leading to the formation of the fusion-pore and the mixing of the protein and lipid components of both membranes have remained topics of active investigation. The crux of the problem involves the fact that the phospholipid bilayer component of biological membranes represents formidable barriers to fusion (2–4). Consequently, synaptic vesicle fusion is viewed as a multistep, highly regulated process involving complexes formed between proteins in the membrane of the vesicle (synaptobrevin) with proteins in the membrane of the presynaptic terminal (syntaxin, SNAP-25) (5–8).

Once close membrane apposition has been established, two radically different models of fusion have been proposed (for review, see (9)). In one model, referred to as direct-fusion, small protein subunits form oligomers that transverse each of the membranes and link across the aqueous space to form a gap-junction-like pore (10,11). Such a fusion pore would first release the vesicle's contents and later facilitate the mixing of the protein and lipid components of vesicle and active zone. In the competing model, referred to as fusion-through-hemifusion, fusion proceeds via sequential merging of the proximal and distal leaflets comprising the membranes (12). First to fuse are the proximal leaflets that face each other across the aqueous space, and form the intermediary called hemi-fusion. During this hemi-fused state, the membranes can exchange lipids and fluorescent markers in the proximal leaflets of the membranes. The distal leaflets remain separate, a fact that hinders the release of the vesicular contents into the extracellular space. Hemi-fusion is thought to represent a stable intermediary in the fusion path of diverse systems, including protein-free bilayers with specific lipid composition (12–14), as well as fusion of viruses with the cell membrane (15). The subsequent merging of the distal leaflets forms the fusion-pore that mediates both release of the vesicular contents and intermixing of lipids and proteins in the distal leaflets of the membranes.

Distinguishing between the models involves solving the three-dimensional structure of the region of contact between vesicles and plasma membrane. In direct-fusion, the region of contact should be composed of two closely apposed membranes, while in the competing fusion-through-hemifusion model only a single hemi-fused membrane should be observed. Determining whether a given area of contact is comprised of a double or single membrane (i.e., ~6 nm or ~12 nm in overall thickness) requires imaging synapses using thin sectioning electron tomography, a method that eliminates the artifact induced by projecting the entire volume of the section onto a single plane (the projection-artifact) and with which it is possible to resolve individual membranes as trilayer structures (the unit-membrane pattern, (16,17)).

In this study, we have applied the general method of conical electron tomography (18,19) to determine the structure of the region of contact in an effort to test predictions from the models. The principal observation was that approximately three-fourths of the vesicles associated (docked) to

Submitted March 10, 2006, and accepted for publication May 31, 2006.

Address reprint requests to G. A. Zampighi, Tel.: 310-206-2883; E-mail: gzampighi@mednet.ucla.edu.

© 2006 by the Biophysical Society

0006-3495/06/10/2910/09 $2.00

doi: 10.1529/biophysj.106.084814

the active zone exhibited small hemi-fused regions. These vesicles were also linked to the plasma membrane by densities shaped as fibrils that might correspond to *trans*-SNARE or core complexes (20). Fully fused vesicles were less frequent (~1 per 10 hemi-fused) and were characterized by pores that appeared as interruptions in a single membrane, which most likely had been hemi-fused. Therefore, the demonstration of hemi-fusion in the region of contact between vesicles and active zone revealed here suggests that the fusion-through-hemifusion model is consistent with how neurotransmitters are released in chemical synapses of the neocortex.

METHODS

Preparation of thin sections

The preparation of the specimens has been described (21–23). We sacrificed three Sprague-Dawley adult rats 90–120 days of age and fixed by perfusion with 3% glutaraldehyde, and 4% paraformaldehyde in 0.2 M cacodylate buffer at pH 7.4. The brains were removed and sliced in a vibrotome in sections 100–150 μm. Tissue from the frontal association and motor neocortices was dissected from the sections and processed for thin sectioning electron microscopy. After OsO_4 post-fixation and block staining, the tissue was embedded in EPON 812. Thin sections of thickness with gray-to-silver interference color (55–80 nm) were cut, collected on 200 mesh grids, and stained with solutions of uranyl and lead citrate. Gold particles, 10 nm in diameter, deposited on the surfaces of the thin sections were used for centering the conical series, estimation of the thin section thickness, and the calculation of preliminary three-dimensional reconstructions.

Glutaraldehyde cross-linking and the Criegee reaction

It is well known that fixatives used in the preparation of thin sectioning electron microscopy react with both the protein and lipid components of tissues. At the concentration used in this study, glutaraldehyde cross-links α-amino groups as well as less reactive groups, such as tyrosinyl (24), guanidyl, imidazolyl, and sulfhydryl groups (25). This means that it will react with most proteins as well as the headgroups of phospholipids, including PE, PS, and PC. In these cross-linking reactions, however, studies using x-ray diffraction methods have shown that the principal features of the three-dimensional structure of proteins remain intact (26). It thus seems unlikely that these reactions could be responsible for changing the overall thickness of the region of contact from ~12 nm to ~6 nm, as would be necessary for a double membrane to appear hemi-fused.

OsO_4 reacts initially with double bonds of unsaturated lipids in the hydrophobic core of bilayers to form monoesters, the Criegee reaction (27,28). These monoesters are further reduced, and liberate oxides of the type $Os(IV)O_4 \cdot nH_2O$, which then migrate to the hydrophilic regions of the phospholipid bilayer. A result of OsO_4 fixation is that all biological membranes, independent of their chemical composition, exhibit a trilayer pattern comprised of two dense bands (the stained surfaces) flanking an electron lucent core (the hydrophobic center), together referred to as the unit-membrane pattern (16,17). Clearly, such a property of the Criegee reaction would enhance, not detract, from the ability to determine whether the region of contact between vesicles and the active zone is comprised of single- or double-unit membranes.

Collection of the conical series

We used the Gatan 650 Single Tilt Rotating Holder (Gatan, Pleasanton, CA) in a FEI Tecnai 12 electron microscope (FEI, Hillsboro, OR) operated at 120 KV to collect 19 conical series. The holder allowed 55° tilts and controlled 5° (72 projections) rotations in the azimuth. The images were collected in a $2k \times 2k$ CCD Gatan camera at 26,000× final magnification (pixel size 0.409 nm). Imaging was carried out using a minimum-dose method: searching was done at 2700× magnification with minimum illumination and the regions of interest imaged by focusing ~2 μm away. The total electron dose was ~800 e/A2, which we previously found decreased the overall thickness of the thin section by ~15% (19).

Centering, alignment, and preliminary three-dimensional reconstructions

To bring the conical series into a common reference system, we selected a specific gold particle as the common center to all images in the series and aligned the entire conical series (72 projections) around this center. After centering, the coordinates of other gold particles (3–8) were recorded for every projection of the series. These values were used to find all orientation parameters (Euler angles and origin position) of the micrographs of the conical series (19). These data were used to calculate the preliminary three-dimensional maps with the weighted back-projection algorithm (29).

Refinement by projection matching

The alignment of the series, based on the manual tracking of the gold particles, was further refined by a strategy of projection matching where the initial projections were iteratively cross-correlated with reprojections of an updating reconstruction. During the computation of the reprojections, we tested incremental adjustments in the three projection parameters, α, β, and γ, and monitored the results by statistical indices based on the variance of the volume. The overall process allowed the determination of the best values for all the shift and orientation parameters and consequently improved both alignment and resolution of the final maps (18,19).

Visualization of the maps

We used the Amira software package (Mercury Computer Systems, San Diego, CA) to visualize entire maps as well as those restricted to docked and fully fused vesicles contained in the synapses. The individual planes comprising the three-dimensional maps were always presented in inverse contrast (Figs. 2, *D–F*; 3, *D–F*; and 5). The reason for this inversion involves the fact that, during visualization, the white pixels represent signal and the black pixels, emptiness. Volume-rendering techniques, where voxels were assigned colors and intensities of light based on a number of user-defined parameters, were used to represent the maps. This type of representation was improved further by segmentation whereby voxels corresponding to vesicles that were hemi-fused or fully fused with the active zone were extracted from each plane. Simply stacking the demarcated regions generated three-dimensional models of individual vesicles as well as neighboring structures, such as the plasma membrane. The maps resulting from these segmentations proved to be exceptional assets in the analysis of the relationships between vesicles that were hemi-fused and fully fused with the active zone.

Resolution of the maps

As there is no direct unequivocal means for accurately ascertaining resolution with electron tomography of nonperiodic specimens, we used two methods and estimated the resolution accordingly. The first method was Fourier Shell Correlation (FSC, (30)), which requires two independent three-dimensional reconstructions. To satisfy this requirement, we split the series into subsets comprised of odd and even numbered images. The subsets were used to reconstruct two independent three-dimensional maps. FSC was computed using either the entire reconstructed volume ($1024 \times 1024 \times 128$ voxel) or small cubic regions ($128 \times 128 \times 128$ voxels) for a local measure of

resolution (19). For computation we have used the EMAN (31) and BSOFT (32) software packages, as well as software developed by one of the members of our research team (S.L.). The resolution was assessed by cutting the FSC curves with thresholds corresponding to five-times the correlation noise (33).

The second method was to measure the thickness of the unit-membrane pattern (18). We used individual planes selected from three refined three-dimensional maps where the pattern was visible throughout the volume. For each map, we selected five planes and in each plane we performed 10–15 measurements using the measuring editor of the Amira package. Since there was significant variability in the distribution of the densities comprising the pattern, we measured regions of the plasma and vesicular membrane where the dense layers appeared equivalent. In these regions, we measured the distance between the centers of the layers (18). This method eliminated the bias in selecting the boundaries of the dense layers. By comparing the resolution between both methods, we have estimated that the resolution of the conical tomographic reconstructions was 3–4 nm (18).

Quantifications

Using the Amira or ImageJ software packages, we measured the length of the active zones in all reconstructions in which they were located (13 out of 19) by measuring the length of a curve line corresponding to the length of thick density in the postsynaptic terminal (densities colored *green*, Fig. 1 *B*). The area of the active zone was calculated by multiplying this length by its thickness estimated from the number of planes in the reconstruction (each plane was .82 nm and the average thickness of the thin sections was 47 $\pm$ 15 nm). Only vesicles the centers of which were contained in the reconstructed volume were included in the count. The total number of vesicles was obtained by examining individual planes comprising the reconstruction to insure that all vesicles were included and none counted twice. The number of docked vesicles was designated as the subset of the total number of vesicles that were in direct contact or located at $<$15 nm from the membrane of the active zone. The number of hemi-fused vesicles corresponds to the subset of docked vesicles where the area of contact with the active zone was comprised of a single unit membrane and measured $\sim$6 nm in overall thickness.

RESULTS

Using conical electron tomography (18,19), we reconstructed chemical synapses from the rat frontal association and motor neocortex prepared for thin sectioning electron microscopy. Key advantages of conical tomography include: 1), elimination of artifacts induced by projecting the entire thickness of the thin section onto a single plane (the projection-artifact); 2), isotropic in-plane resolution (3–4 nm)—approximately two orders-of-magnitude higher than that achieved by optical methods; 3), high throughput; and 4), elimination of the need to impose symmetry or use averaging methods to increase signal/noise ratios.

Of the 19 synapses reconstructed, 13 maps contained active zones. These three-dimensional maps were studied by rendering their entire volume ($\sim$0.1 μm^3) (Fig. 1 *A*), by visualizing their individual planes (Figs. 2; 3, *D–F*; 4, *D–F*; and 6, *A–C*), and by segmenting the volumes of plasma membranes and hemi-fused as well as fully fused vesicles (Figs. 1 *B*; 3, *A–C*; 4, *A–C*; and 5). These visualization methods showed that the presynaptic terminal contained the characteristic vesicles described in previous studies of chemical synapses using conventional thin section electron microscopy (34–36). These synaptic vesicles were clustered at the

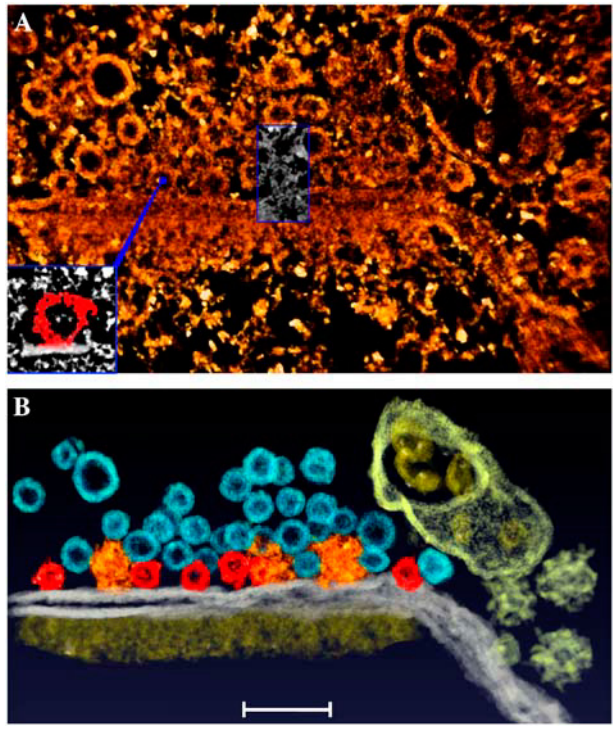

FIGURE 1 Three-dimensional map of a synapse visualized by volumetric rendering and density segmentation. (*A*) The synapse is comprised of a presynaptic (*upper half*) and a postsynaptic (*lower half*) terminal. Spherical profiles of different diameters represent the membranous organelles in the presynaptic terminal. The synaptic vesicles appear as small spheres that cluster at the active zone, which itself faces a layer of density associated with the postsynaptic plasma membrane. Other membrane-bound organelles include a group of three coated vesicles, a coated pit (*lower right side*) and a large endosome with vesicles inside the lumen (*upper right corner*). Docked synaptic vesicles are closest to the membrane of the active zone. This reconstruction has six docked vesicles. The rectangle at the center of the panel encloses the volume of the docked vesicle that is shown in Fig. 2. The inset shows an individual plane of another docked vesicle. To underscore the closeness of the region of contact, the vesicle was colored red and the plasma membrane white. The volume of the reconstruction was $\sim$0.1 μm^3 and the resolution, estimated from the unit-membrane pattern, $\sim$4 nm. (*B*) The densities of two of the different membranous organelles were extracted (segmented) and reconstructed independently (*color-coded*). The parallel white bands represent the pre- and postsynaptic plasma membranes separated by the extracellular space. The thick brown layer associated to the plasma membrane represents the postsynaptic densities that define the active zone in the presynaptic terminal. The three orange particles associated to the plasma membrane between the vesicles belong to the presynaptic web (49–51). Depending on their distance to the active zone, the synaptic vesicles were located at $\sim$15 nm from the active zone (docked and in *red*) or deeper within the terminal (in *blue*). (Note that the viewing angle induces the illusion that some of the red vesicles seem farther from the active zone while some of the blue vesicles seem closer than the 50-nm separation.) The organelles colored yellow outside the active zone include a coated pit, three coated vesicles, and a large endosome with vesicles in its lumen. The distinctive structure in conjunction with its location outside the active zone allowed us to identify these profiles as unambiguously belonging to classical clathrin-related retrieval apparatuses. Bar: 265 nm.

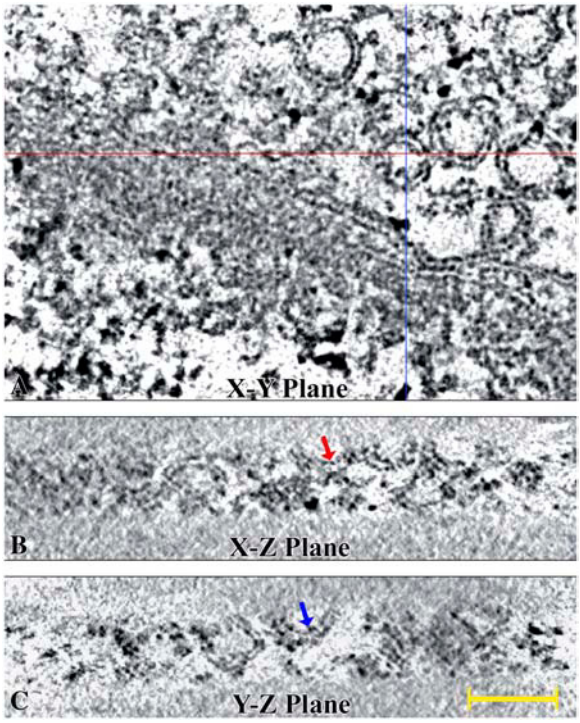

FIGURE 2 The unit membrane pattern is resolved along all directions. (*A*) The unit membrane pattern is comprised of two dense layers flanking an electron lucent center, the whole of which measures ~6 nm in overall thickness. The pattern is seen in the membranes of the pre- and postsynaptic terminals and vesicles. The red and blue lines indicate the approximated location of planes oriented perpendicular to the *x*,*y* plane. (*B*, *C*) The unit membrane pattern is also visualized comprising the membrane of synaptic vesicles viewed in the *x*,*z* and *y*,*z* planes. Since the overall thickness of the pattern is ~6 nm, it follows that the resolution of the map (3–4 nm) allowed our resolving the pattern in all directions. The red and blue arrows point to the same vesicle viewed in the two planes. Incomplete vesicles appear as hemicups, an effect resulting from sectioning. All panels in the figure are individual planes presented in positive contrast. Bar: 50 nm.

active zone (37), the region of the presynaptic membrane facing the thick layer of densities associated to the postsynaptic membrane (*brown*, Fig. 1 *B*). Other organelles such as coated pits, coated vesicles, and large membranous sacs, called endosomes, were also present in the terminal, but these were located outside the region defined in this study as the active zone (*yellow*, Fig. 1 *B*).

We relied on the unit membrane pattern (16,17), representing the phospholipid bilayer structure to estimate the resolution achieved in the maps. To perform this task, we sectioned the reconstructed volume along orthogonal directions (*x*,*y*; *x*,*z*; and *y*,*z* planes). We measured the pattern from the center of the stained layers in the *x*,*y* (Fig. 2 *A*), *y*,*z* (Fig. 2 *B*), and *y*,*z* planes (Fig. 2 *C*), and determined an overall thickness of 6.1 ± 0.25 nm. The resolution of the maps was thus ~3 nm, and was unaffected by either the distance of features from the center of the map or their orientation with respect to the tilt axis.

Having determined that the resolution of the maps was 3–4 nm in all directions, we proceeded to analyze the presynaptic terminals by counting the total number of vesicles and by measuring their diameter and the area of active zone to which they were associated. The diameter of these vesicles had a bimodal distribution: In four reconstructions, vesicle diameters measured 50 ± 7 nm (mean ± SD, $n = 16$), while in the remaining 15 it was 62 ± 5 nm ($n = 18$). Whether or not this bimodal distribution reflects functional differences among the synapses in the region (inhibitory/exhibitory) will require reconstructions of synapses that have been characterized functionally previous to chemical fixation.

We counted a total of 778 vesicles, 53 of which (or ~7% of the total) were docked to ~0.4 μm^2 of active zone (Table 1). A vesicle was considered docked when its membrane was within 15 nm of the active zone. To distinguish between the direct-fusion and the fusion-through-hemifusion models, we then determined whether double or single membranes comprised the region of contact that docked vesicles established with the active zone. We found that regions comprised of a single membrane (hemi-fusion) could be seen in 42 of these 53 vesicles (or ~74% of docked vesicles). In the remaining 11 docked vesicles, two closely apposed unit membranes comprised the regions of contact. These observations indicate that the overwhelming majority of docked vesicles were hemifused to the membrane of the active zone.

We then proceeded to study the region of contact of the 42 vesicles that contained hemi-fused regions along the *z*-direction (depth). The region of contact measured ~15 nm in total depth and exhibited a complex structure. Two-thirds (~10 nm) of the area of contact was comprised of two closely apposed unit membranes (Fig. 3, *D* and *G*), while the remaining region (~5 nm) was hemi-fused and comprised of a single unit membrane (*vertical arrows*, Fig. 3, *E*, *F*, *H*, and *I*). Using 50 nm for the diameter of an average synaptic vesicle, we estimated that the entire region of contact occupied ~2% and that the smaller hemi-fused region occupied only

TABLE 1 Summary of information obtained from the reconstructions of active zones in rat neocortex synapses

Reconstruction	Active zone length (nm)	Active zone area (nm^2)	Total # of vesicles	Docked vesicles*	Hemi-fused vesicles
5_20	546	25,933	195	9	6
5_21	260	7279	51	3	1
5_27	480	19,525	57	2	1
5_28a	446	12,510	39	2	1
7_23	1021	44,920	74	2	2
7_26	366	14,623	45	3	3
7_30	942	65,542	54	4	4
8_03	654	40,732	77	5	3
8_13	879	62,633	44	6	5
8_14	462	18,522	31	5	5
8_16	700	35,273	18	6	6
8_17	417	12,696	23	3	2
8_16b	710	44,274	70	3	3

*Including the docked vesicles that are hemi-fused.

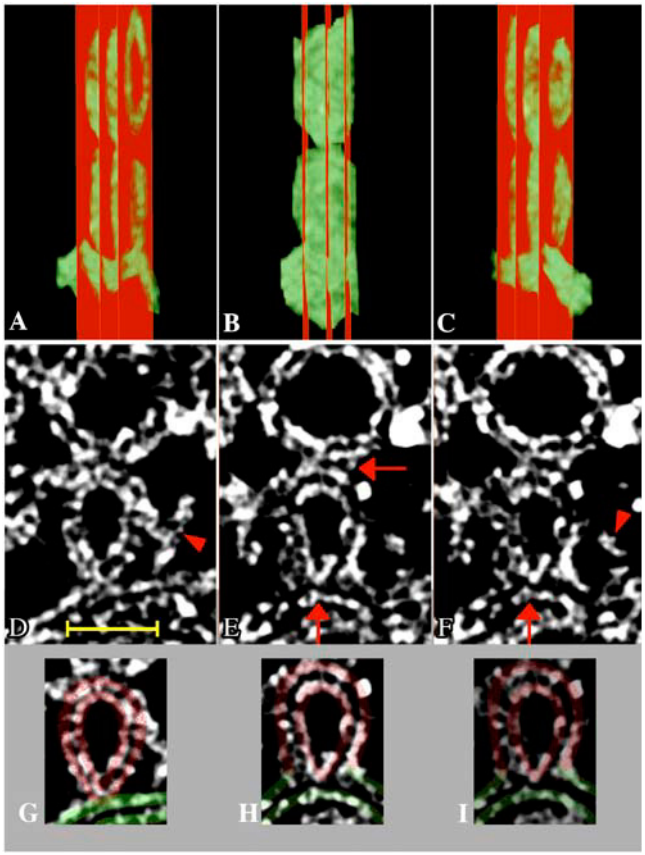

FIGURE 3 Vesicles docked with the active zone. (*A–C*) Small volume cropped from the reconstruction in Fig. 1 *A* (*rectangle*). The densities correspond to a vesicle docked to the plasma membrane on one side and associated to an adjacent vesicle on the other. The rectangles slicing through the densities indicate the approximate location of the three planes that were selected to illustrate the structure of this docked vesicle. Two side views (*A*, *C*) and one edge-on view (*B*) of the densities, colored green, are shown. (*D–F*) Images of individual planes along the z-direction (depth) indicated by the rectangles in the upper panels. (*G–I*) The same images cropped to include images of only a small region of the active zone (*green lines*) and a docked vesicle (*red lines*). The densities were displayed in reverse contrast. (*D*, *G*) (plane #46) Shows that the side contacting the plasma membrane exhibited a pronounced curvature and was comprised of two closely apposed unit membranes (*red* and *green* in *G*). The side contacting the adjacent vesicle immediately above was less deformed but it was also comprised of two closely apposed unit membranes. The docked vesicle is linked to the plasma membrane by a long fibril (*arrowhead*) and a shorter fibril, oriented perpendicular to each other. (*E*, *F*, *H*, and *I*) (planes #50 and #52) Shows planes through the hemi-fused region. The side contacting the plasma membrane is comprised of a single unit membrane. This feature is also underscored in panels *H–I* by the fact that at the region of contact (*vertical arrows*, *E* and *F*), the unit membrane is comprised of a red line (the distal leaflet of the vesicle) and a green line (the distal leaflet of the active zone). The docked vesicle is thus hemi-fused to the active zone but not with the vesicle immediately above. The densities connecting this docked vesicle to the active zone (*arrowheads*, *D* and *F*) might represent a *trans*-SNARE complex. Bar: 50 nm.

~0.2% of the vesicle's area. Therefore, the region of contact between docked vesicles and the active zone includes sections of close membrane apposition (Fig. 3, *D* and *G*), and hemi-fusion (Fig. 3, *E*, *F*, *H*, and *I*).

Three additional features characterized the region of contact, all of which have been proposed as properties leading to the opening of the fusion pore in the fusion-through-hemifusion model. The first was a pronounced curvature that, in the plane, gave the docked vesicle a triangular appearance (Fig. 3, *D–I*) and, in three dimensions, a pear shape. The second was a shallower curvature in the plasma membrane toward the vesicle; since the two curvatures were of the opposite sign, the region of contact appeared as a stalk (Fig. 3, *D* and *G*). The third was the existence of densities linking the hemi-fused side with the active zone (*arrowheads*, Fig. 3, D and *F*). These densities appeared either as fibrils or as rings of ~15 nm in diameter (*arrowhead*, Fig. 3 *F*). The fibrils were oriented perpendicularly, with the longer fibril (~30 nm) attached to the plasma membrane (*arrowhead*, Fig. 3 *D*) and the shorter fibril (~8.5 nm) attached to the vesicle. The finding of these types of densities is consistent with the idea that protein complexes bring vesicles into close proximity with the active zone.

Our study also identified four vesicles that were fully fused and appeared as small dimples in the membrane of the active zone (Figs. 4 and 5). The principal attribute of fully fused vesicles was a prominent pore that appeared as an interruption, (3–8 nm) in width, of the membrane at the region of contact. The pore was patent when examining individual planes of the region (*arrow*, Fig. 4, *E* and *F*) as well as when the volume of the fully fused vesicles was segmented and visualized by surface triangulation (*arrow*, Fig. 5 *D*). Using this visualization method, the pore was found to open toward the perimeter of the hemi-fused region rather than at its center (*arrow*, Fig. 4 *E*). We estimated a ratio of approximately one fully fused vesicle to every ~10 hemi-fused vesicles (42:4). Despite this expectedly low frequency (see discussion), their observation in four independent reconstructions indicates that they appear to be a normal feature of synapses that have not been stimulated previous to fixation. Once again, conventional thin sectioning will make visualization of a pore of such dimensions impossible.

It was necessary to ask why hemi-fused vesicles have not been seen in studies using conventional electron microscopy (38). As stated above, the hemi-fused region occupies a small fraction of the total thickness of the section (~1/8). To test the possibility that projection artifacts might be responsible for the failure, we compared individual planes gathered from hemi-fused vesicles (Fig. 6, *A–C*) with projections of the entire volume (64 consecutive planes or ~50 nm in thickness) of these same vesicles (Fig. 6, *D–F*). Analysis of the individual planes showed the two defining properties of hemi-fused vesicles at the region of contact: the merging of the proximal leaflets and the deformation of the membranes (*red arrows*, Fig. 6, *A–C*). When examining projections of these regions of contact, however, the images were quite different (Fig. 6, *D–F*). In two projected images, diffuse densities linking the vesicle to the plasma membrane replaced the hemi-fused region (*yellow arrows*, Fig. 6, *D* and *F*). In another projection, the

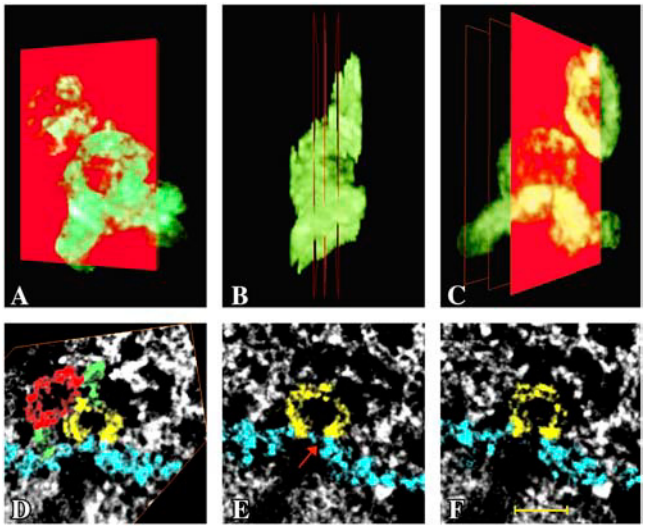

FIGURE 4 Vesicles fully fused with the active zone. (*A–C*) Small volume containing densities of a vesicle associated to the plasma membrane on one side and to an adjacent vesicle on the other. In contrast to the volume in Fig. 3, this docked vesicle is fully fused to the plasma membrane. The next vesicle in the chain was hemi-fused to the dimple created by the fusion event. The rectangles cutting through the densities indicate the approximate location of the planes that were selected to illustrate the structure of the region. The densities (*green*) are shown in side views (*A*, *C*) and an edge-on view (*B*). The upper vesicle is located to the side of the one fused to the plasma membrane (*C*). In the lower panels, to assist in the visualization of the fusion event, the plasma membrane was colored blue, the fully fused vesicle was colored yellow, and the hemi-fused vesicle was colored red. (*D*) An oblique plane indicating that the docked vesicle is in fact fully fused to the plasma membrane. A key feature of this obliquely sectioned plane is the region of contact between the vesicle in the second tier (*red*) and the dimple created by the fusion event (*yellow*), as illustrated by the mixing of the colors. Measurements of this region along the *x*,*y* plane at different points in the *z* direction have been as low as ~6 nm, suggesting that there may be areas of hemi-fusion at the region of contact between these two vesicles. Panels *E* and *F* (planes #13 and 15) show a discontinuity of the membrane (*arrow*) that represents the pore spanning the entire region of contact between the fully fused vesicle and the active zone. It is important to note that due to the pore, the previously independent vesicle must now be considered as an extension of the plasma membrane inside the terminal. Bar: ~50 nm.

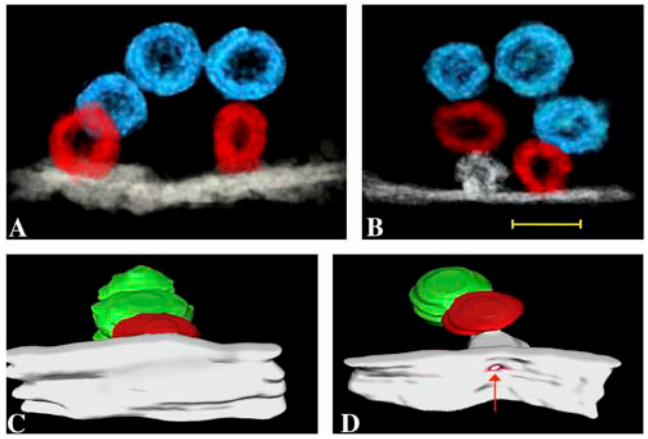

FIGURE 5 Vesicles deeper in the terminal are arranged in chains. Synaptic vesicles establishing close contacts formed chains that interlinked vesicles docked to the active zone. (*A*) Segmentation comprised of five synaptic vesicles (*red* and *blue*) and the nearest region of the active zone (*white band*). The vesicles that are docked to the active zone are hemi-fused (*red*), while the vesicles comprising the crook of the arch, though they are in direct contact, do not hemi-fuse (*blue*). The center of the arch appears empty but in the complete reconstruction, it is in fact occupied by particles of the synaptic grid structure. This vesicular chain was segmented from the map in Fig. 1 *A*, where the synaptic grid particles are represented by the orange volumes. (*B*) Vesicular chain interlinking a fully fused vesicle (*white*) to a hemi-fused vesicle (*red*). A key feature of this chain is that the next tier vesicle (*red*) hemi-fused at the dimple created by the previous fusion event. Panels *C* and *D* compare reconstructions of the region of contact of a hemi-fused vesicle (*C*) and a fully fused vesicle (*D*). Both views show the region of contact viewed from the extracellular space. The region of contact of the fully fused vesicle exhibits a pore (*arrow*). The segmentations of panels *C* and *D* were visualized using triangulation instead of volume-rendering methods. Bar: 60 nm.

docked vesicle was barely visible (Fig. 6 *E*). Since projection images mimic imaging by conventional electron microscopy, this simulation indicates that features smaller than the thickness of the section (~50 nm), such as an 5–6 nm diameter hemi-fused region, cannot be resolved with this method.

We also explored the possibility that hemi-fused regions could exist in areas of membrane contact outside the active zone. To test this possibility, we have examined the area of contact established by the 778 synaptic vesicles seen in our three-dimensional maps. Regions where two or more vesicles come into contact are ideally suited for the study because they existed in large numbers (many vesicles contact several neighbors) and their interacting membranes exhibit high curvature. Our analysis of these regions did not yield a single hemi-fused region.

Based on these considerations, we thus suggest that the hemi-fused state is a key structural feature of synaptic vesicles that were docked with the active zone in the rat neocortex.

DISCUSSION

Analysis of three-dimensional maps calculated using conical tomography have allowed the identification of novel structural properties of chemical synapses that have escaped detection in studies using conventional imaging methods with the electron microscope due primarily to technical reasons, such as the projection-artifact. Among these properties we highlight: 1), that vesicles docked to the active zone are hemi-fused (Figs. 3 and 7 *B*); and 2), that the pore in fully fused vesicles transverses a single membrane (Figs. 4 and 7 *C*). We found 42 vesicles in 13 reconstructions that are hemi-fused with the plasma membrane on one side and contiguous but not hemi-fused on the other. In all 778 vesicles studied, no instance of hemi-fusion was found among vesicles removed from the active zone. It is therefore possible to assert with some confidence that our observations are not due to artifacts resulting from chemical fixatives, as it is difficult to propose how any artifact could consistently affect only one half of the

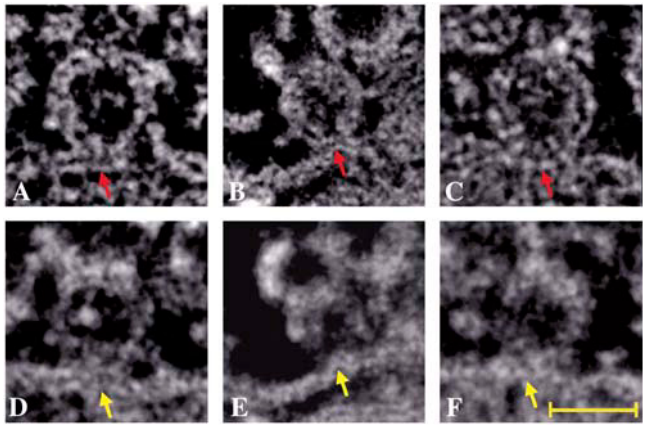

FIGURE 6 Projecting the volume of the section on a single plane prevents visualization of the hemi-fused regions in docked vesicles. (*A–C*) Individual planes from different three-dimensional reconstructions of synaptic vesicles that are hemi-fused to the active zone (*red arrows*). (*D–F*) Projection calculated by averaging the volume of 64 planes or ~50 nm along the *z*-direction (thickness). Instead of a hemi-fused region comprised of single unit membranes, the vesicles and regions of contact become diffuse (*yellow arrows*). In one example (*E*), the projection of the vesicle hemi-fused to the active zone is barely visible. Another vesicle, not present in the individual plane in panel *B*, is now the most prominent vesicle in the projected image. Therefore, the projection artifact would make visualization of a small feature, such as the hemi-fused region of docked vesicles, impossible in images gathered using conventional thin-sectioning electron microscopy. All images are in reverse contrast. Bar: 50 nm.

synaptic vesicle in contact with the active zone, and fail to affect the areas of contact among the vesicles themselves.

The three-dimensional structure of vesicles docked to the active zone allows us to distinguish between competing models of fusion pore formation, the key intermediary leading to neurotransmitter release and synaptic transmission. In the model of direct-fusion, it is proposed that a gap-junction-like pore transverses two apposing membranes and releases the vesicle's contents (for review, see (6)). This model gives rise to the prediction that the region of contact should be comprised of two intimately apposed unit-membranes and measure ~12 nm in overall thickness. In the fusion-through-hemifusion model, it is proposed that fusion proceeds via the sequential merging of first the proximal and then the distal leaflets of the apposing membranes. The state created by the hemi-fusion of the proximal leaflets hinders release of the vesicular contents into the extracellular space. Only after the distal leaflets have merged, can the pore open and the vesicular contents be released, completing the mixing of lipids and proteins (for review, see (9)). This model gives rise to the prediction that the region of contact should partially consist of a single unit membrane, measuring ~6 nm in overall thickness, and that the fusion pore should traverse a single unit membrane (Fig. 7).

The three-dimensional maps gathered in this study allowed us to test the predictions derived from these two models. Analysis of the individual planes of the region of contact of hemi-fused vesicles indicated that a single unit membrane was present in the region of contact (Fig. 3, *D–F*). Moreover, similar analysis performed at the region of contact of vesicles that were fully fused with the active zone showed that their fusion-pores span only this single membrane (Fig. 4, *D–F*). We thus suggest, based on our reconstructions, that the fusion-through-hemifusion or stalk-model reflects the structure of docked and fully fused vesicles more accurately than the direct-fusion model.

The hemi-fused region occupied only a small part of the region of contact between docked vesicles and the active zone (Fig. 3, *E* and *F*). Using the figure of 50 nm for the diameter of an average synaptic vesicle, we estimated that the smaller hemi-fused region occupied only ~0.2% of the vesicle's area. The small dimension of the hemi-fused region with respect to the section's thickness (40–50 nm) additionally helps to explain why studies using conventional thin sectioning electron microscopy have failed to resolve this critical structural characteristic of docked vesicles.

It is useful to express the number of docked and hemi-fused vesicles as a function of the area of the active zone (Table 1). Since 53 vesicles (~7% of the total) were docked to ~0.4 μm^2 of active zone, we estimated that the density of docked vesicles should be ~130/μm^2. To further understand the significance of our measurements, we can express this density as an average synapse from the 13 maps (~0.6 μm in length and, assuming circular geometry, ~0.28 μm^2 of active zone area). From the proportionality between vesicles and the active zone established experimentally, we can further conclude that such a synapse would have ~37 docked and ~28 hemi-fused vesicles (Table 1). This prediction marks a first estimate of docked vesicles expressed per unit area of active zone.

The three-dimensional structure of the vesicles docked to the active zone contains features pertaining to the hypothesis that populations (i.e., pools) of vesicles with distinct

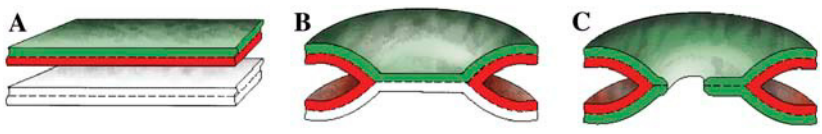

FIGURE 7 Some of the states leading to the formation of the fusion pore (modified from (52)). Three different states of the area of contact between the membranes of synaptic vesicles and the active zone are illustrated in the panels. (*A*) Region of close membrane apposition where both membranes are separated by a small aqueous space. This state is proposed in both the direct-fusion and the fusion-through-hemifusion models. (*B*) Region of contact exhibiting hemi-fusion. In this state, the proximal leaflets (*red*) merge and the distal leaflets (*green* and *white*) form the bilayer. This state is predicted by the fusion-through-hemifusion model and was frequently seen in the vesicles docked to the active zone. (*C*) Fusion-pore at the perimeter of the hemi-fused region. In this state, both the proximal (*red*) and distal (*green*) leaflets of both membranes have merged. This fusion pore was infrequently seen in our study. For clarity, the leaflets of the phospholipid bilayer of the upper membrane were colored green (distal) and red (proximal).

functional properties exist in the presynaptic terminal (39,40). Conventional electron microscopy studies have hitherto identified no significant structural feature beyond that of distance from the active zone, which can be used to distinguish among vesicles in the terminal. Yet numerous functional studies indicate that synaptic vesicles can be separated into pools: those that are immediately available on stimulation, and those that release only upon intense stimulation (for review, see (41)). The finding of hemi-fusion marks the first instance of an additional characteristic directly relevant to this hypothesis: It follows simply that vesicles hemi-fused to the active zone may comprise the immediately-releasable pool (39,41).

Finally, the structure of docked vesicles supports the hypothesis that complexes comprised of SNARE proteins link synaptic vesicles to the active zone. Our observations that densities appearing as filaments or rods connecting hemi-fused vesicles with the plasma membrane strongly support this prediction (*arrowheads*, Fig. 3, *D* and *F*). Our observations offer no inconsistencies with atomic models of the *trans*-SNARE complexes determined by x-ray diffraction methods (42); however, a precise identification of individual SNAREs will require reconstructions of synapses where one or several of these proteins have been manipulated or knocked out. Despite these limitations in identifying individual SNAREs, our observations nonetheless provide direct evidence that complexes that form in vitro by mixing liposomes and purified SNAREs (43) could also exist in a synaptic environment.

In conclusion, our observations add docked synaptic vesicles to a long list of systems, in which hemi-fusion has been observed as a normal constituent of membranes in close apposition. Along with protein-free bilayers (12–14), SNARE-containing liposomes (44–46), viral fusion (2), SNARES that are ectopically expressed in cells (47), and physiological homotypic fusion of yeast vacuoles (48), docked synaptic vesicles also exhibit regions of contact where sequential merging of proximal and distal leaflets of apposing membranes lead to a fusion pore traversing only a single unit membrane. As with its observation elsewhere, the finding of hemi-fusion in synapses has profound consequences on our understanding of the system as a whole, not the least of which are its impact on the model of vesicular fusion, and its implication on the organization of functional pools.

We thank Drs. F. Schweitzer, C. Gundersen, and A. Grinnell for comments during the preparation of the manuscript.

This work was supported by grant No. EY-04110 as well as funds from the Foundation to Prevent Blindness (to G.Z.); grant No. GM-27278, from Philip Morris USA and Philip Morris International (to S.S.); FIRST 2001 (to S.L.); and grant No. DK44602 (to E.W).

REFERENCES

1. Katz, B. 1971. Quantal mechanism of neural transmitter release. *Science.* 173:123–126.
2. Chernomordik, L. V., and M. M. Kozlov. 2003. Protein-lipid interplay in fusion and fission of biological membranes. *Annu. Rev. Biochem.* 72:175–207.
3. Cohen, F. S., and G. B. Melikyan. 2004. The energetic of membrane fusion from binding, through hemifusion, pore formation, and pore enlargement. *J. Membr. Biol.* 199:1–14.
4. Malinin, V. S., and B. R. Lentz. 2004. Energetics of vesicle fusion intermediaries: comparison of calculations with observed effects of osmotic and curvature stresses. *Biophys. J.* 86:2951–2964.
5. Sudhof, T. C. 1995. The synaptic vesicle cycle: a cascade of protein-protein interactions. *Nature.* 375:645–653.
6. Jahn, R., and T. C. Sudhof. 1999. Membrane fusion and exocytosis. *Annu. Rev. Biochem.* 68:863–911.
7. Jahn, R., T. Lang, and T. C. Sudhof. 2003. Membrane fusion. *Cell.* 112: 519–533.
8. Li, L., and L.-S. Chin. 2003. The molecular machinery of synaptic vesicle exocytosis. *Cell. Mol. Life Sci.* 60:942–960.
9. Chernomordik, L. V., and M. M. Kozlov. 2005. Membrane hemifusion: crossing a chasm in two leaps. *Neuron.* 123:375–382.
10. Peters, C., M. J. Bayer, S. Buhler, J. S. Andersen, M. Mann, and A. Mayer. 2001. Trans-complex formation by proteolipid channels in the terminal phase of membrane fusion. *Nature.* 409:581–588.
11. Han, X., C. T. Wang, J. Bai, E. R. Chapman, and M. B. Jackson. 2004. Transmembrane segments of syntaxin line the fusion pore if Ca^{2+}-triggered exocytosis. *Science.* 304:289–292.
12. Chernomordik, L., A. Chanturiya, J. Green, and J. Zimmerberg. 1995. The hemifusion intermediary and its conversion to complete fusion: regulation by membrane composition. *Biophys. J.* 69:922–929.
13. Cohen, F. S., J. Zimmerberg, and A. Finkelstein. 1980. Fusion of phospholipids vesicles with planar phospholipids bilayer membranes. II. Incorporation of a vesicular membrane marker into the planar membrane. *J. Gen. Physiol.* 75:251–270.
14. Lee, J., and B. R. Lentz. 1997. Evolution of lipidic structures during model membrane fusion and the relation of this process to cell membrane fusion. *Biochemistry.* 36:6251–6259.
15. Kemble, G. W., T. Danieli, and J. M. White. 1994. Lipid-anchored influenza hemagglutinin promotes hemifusion, not complete fusion. *Cell.* 76:383–391.
16. Robertson, J. D. 1959. The ultrastructure of cell membranes and their derivatives. *Biochem. Soc. Symp.* 16:3–43.
17. Robertson, J. D. 1987. The early days of electron microscopy of nerve tissue and membranes. *Int. Rev. Cytol.* 100:129–201.
18. Lanzavecchia, S., F. Cantele, P. L. Bellon, L. Zampighi, M. Kreman, E. M. Wright, and G. A. Zampighi. 2005. Conical tomography of freeze-fracture replicas: a method for the study of integral membrane proteins inserted in phospholipid bilayers. *J. Struct. Biol.* 149:87–98.
19. Zampighi, G. A., L. Zampighi, N. Fain, E. M. Wright, F. Cantele, and S. Lanzavecchia. 2005. Conical Tomography II: a method for the study of cellular organelles in thin sections. *J. Struct. Biol.* 151:263–274.
20. Sollner, T., S. W. Whiteheart, M. Brunner, H. Erdjument-Bromage, S. Geromanos, P. Tempst, and J. E. Rothman. 1993. SNAP receptors implicated in vesicle targeting and fusion. *Nature.* 362:318–324.
21. Zampighi, G. A., J. M. Corless, and J. D. Robertson. 1980. On gap junction structure. *J. Cell Biol.* 86:190–198.
22. Zampighi, G. A., J. E. Hall, G. R. Ehring, and S. A. Simon. 1989. The structural organization and protein composition of lens fiber junctions. *J. Cell Biol.* 108:2255–2275.
23. Zampighi, G. A., and R. S. Fisher. 1997. Polyhedral protein cages encase synaptic vesicles and mediate their docking to the pre-synaptic membrane. *J. Struct. Biol.* 119:347–359.
24. Bowes, J. H., and C. W. Carter. 1968. The interaction of aldehydes with collagen. *Biochim. Biophys. Acta.* 168:322–341.
25. Habeeb, A. F., and R. Hiramoto. 1968. Reaction of proteins with glutaraldehyde. *Arch. Biochem. Biophys.* 126:1–16.
26. Hopwood, D. 1972. Theoretical and practical aspects of glutaraldehyde fixation. *Histochem. J.* 4:99–127.
27. Criegee, R. 1936. Osmium saure-ester als mischerproducte beir oxidation. [Osmium acid-ester as byproduct of oxidation.]. *Ann. Chem.* 522:75–96.

28. Criegee, R., B. Marchand, and H. Wannowius. 1942. Zur kentniss der organischer osmium-verbinguen gen. [On organic osmium compounds.]. *Ann. Chem.* 550:99–133.

29. Radermacher, M. 1992. Weighted back-projection methods. *In* Electron Tomography. J. Frank, editor. Plenum Press, New York.

30. van Heel, M. 1987. Similarity measures between images. *Ultramicroscopy.* 21:95–100.

31. Ludtke, S. J., P. R. Baldwin, and W. Chin. 1999. EMAN: semiautomated software for high-resolution single particle reconstructions. *J. Struct. Biol.* 128:82–97.

32. Heyman, B. J. 2001. BSOFT: image and molecular processing in electron microscopy. *J. Struct. Biol.* 133:156–169.

33. Radermacher, M. 1988. Three-dimensional reconstruction of single particles from random and non-random tilt series. *J. Electron Microsc. Tech.* 9:359–394.

34. Sjostrand, F. S. 1953. Ultrastructure of retinal rod synapses of Guinea-pig eye. *J. Appl. Phys.* 24:1422–1423.

35. Palay, S. L., and G. E. Palade. 1955. The fine structure of neurons. *J. Biophys. Biochem. Cytol.* 1:68–88.

36. Gray, E. G. 1963. The granule cells, mossy synapses and Purkinje spine synapses of the cerebellum: light and electron microscope observations. *J. Anat.* (*Lond.*). 97:101–106.

37. Couteaux, R. 1961. Principaux criteres morphologiques et cytochimiques utilisables aujourd'hui pour definir les divers types de synapses. [Principal morphological and cytochemical criteria to define the diverse types of synapses.]. *Acta Neurophysiol.* 3:143–173.

38. Heuser, J. E., and T. S. Reese. 1981. Structural changes after transmitter release at the frog neuromuscular junction. *J. Cell Biol.* 88:564–580.

39. Delgado, R., C. Maureira, C. Oliva, Y. Kidokoro, and P. Labarca. 2000. Size of vesicular pools, rates of mobilization, and recycling and neuromuscular synapses of a *Drosophila* mutant, *shibire*. *Neuron.* 28: 941–953.

40. Schikorski, T., and C. F. Stevens. 2001. Molecular correlates of functionally defined synaptic vesicle populations. *Nat. Neurosci.* 4: 391–395.

41. Rizzoli, S. O., and W. J. Betz. 2005. Synaptic vesicle pools. *Nat. Neurosci. Rev.* 6:57–69.

42. Sutton, R. B., D. Fasshauser, R. Jahn, and A. T. Brunger. 1998. Crystal structure of a SNARE complex involved in synaptic exocytosis at 2.4 Å resolution. *Nature.* 395:347–353.

43. Weber, T., B. V. Zemelman, J. A. McNew, B. Westermann, M. Gmachl, F. Parlati, T. H. Sollner, and J. E. Rothman. 1998. SNAREpins: minimal machinery for membrane fusion. *Cell.* 92: 759–772.

44. Lu, X., F. Zhang, J. A. McNew, and Y.-K. Shin. 2005. Membrane fusion induced by neuronal SNAREs transits through hemifusion. *J. Biol. Chem.* 280:30538–30541.

45. Xu, Y., F. Zhang, Z. Su, J. A. McNew, and Y. K. Shin. 2005. Hemifusion in SNARE-mediated membrane fusion. *Nat. Struct. Mol. Biol.* 12:417–422.

46. Dennison, M. S., M. E. Bowen, A. T. Brunger, and B. R. Lentz. 2006. Neuronal SNAREs do not trigger fusion between synthetic membranes but do promote PEG-mediated membrane fusion. *Biophys. J.* 90:1661–1675.

47. Giraudo, C. G., C. Hu, D. You, A. M. Slovic, E. V. Mosharov, D. Sulzer, T. J. Melia, and J. E. Rothman. 2005. SNAREs can promote complete fusion and hemifusion as alternative outcomes. *J. Cell Biol.* 170:259–260.

48. Reese, C., F. Heise, and A. Mayer. 2005. Trans-SNARE pairing can precede a hemifusion intermediary in intracellular membrane fusion. *Nature.* 436:410–414.

49. Bloom, F. E., and G. K. Aghajanian. 1966. Cytochemistry of synapses: a selective staining method for electron microscopy. *Science.* 154: 1575–1577.

50. Pfenninger, K., K. Akert, H. Moor, and C. Sandri. 1972. The fine structure of freeze-fractured presynaptic membranes. *J. Neurocytol.* 1: 129–149.

51. Phillips, G. R., J. K. Huang, Y. Wang, H. Tanaka, L. Shapiro, W. Zhang, W.-S. Shan, K. Arndt, M. Frank, M. A. Gawinowicz, and D. R. Colman. 2001. The presynaptic particle web: ultrastructure, composition, dissolution, and reconstitution. *Neuron.* 32:63–77.

52. Kozlovsky, Y., L. V. Chernomordik, and M. M. Kozlov. 2002. Lipid intermediaries in membrane fusion: formation, structure, and decay of the hemifusion diaphragm. *Biophys. J.* 83:882–895.